Chapter 4
Modeling and Simulation

Yutaka Kaneko

This chapter is devoted to recent developments in mathematical modeling and computer simulation of copper electrodeposition. We focus our attention on continuum models and kinetic Monte Carlo simulations for shape evolution and the effects of additives on copper deposition, especially the filling of small features in microelectronics. The modeling, mathematical treatments, and simulation results are reviewed with brief summaries of efficient numerical algorithms. Fast computing and prospects of simulation research are also discussed.

4.1 Introduction

Copper electrodeposition has attracted a great deal of attention since IBM announced the replacement of conventional vapor deposition of aluminum with copper electrodeposition for the production of LSI interconnects [1]. The dual damascene process is now a central technique for the fabrication of three-dimensional (3D) LSI circuits. An important requirement for the success of this process is the capacity to fill submicron features such as via holes and trenches completely without voids or seams. This process is called "superfilling" or "superconformal filling." It has been found experimentally that superfilling is achieved by the synergistic effects of different kinds of additives, and the optimal deposition conditions have been explored.

Mathematical modeling and numerical simulations are indispensable means of research to understand the underlying chemistry from a microscopic point of view and to determine the optimal conditions for practical applications. There are two types of modeling for copper electrodeposition. The first type is based on

Y. Kaneko (✉)
Department of Applied Analysis and Complex Dynamical Systems Graduate School of Informatics, Kyoto University, Yoshida-Honmachi, Sakyo-ku, Kyoto 606-8501, Japan
e-mail: kaneko@acs.i.kyoto-u.ac.jp

K. Kondo et al. (eds.), *Copper Electrodeposition for Nanofabrication of Electronics Devices*, Nanostructure Science and Technology 171, DOI: 10.1007/978-1-4614-9176-7_4,

"continuum models" in which the physical quantities are expressed in terms of continuous variables. The basic equations are partial differential equations. The second type is "molecular simulation" such as Monte Carlo (MC) and molecular dynamics (MD) computations in which ions and molecules are treated as particles. In this chapter, we overview the recent developments of these two types of simulation for copper electrodeposition to understand the present status of sophistication.

This chapter is organized as follows. The next section is the brief review of the numerical simulations based on continuum models. Section 4.2.1 is devoted to the mathematical models for superfilling. The basic ideas and mathematical formulas of the diffusion-consumption theory [1–5], the recent theory of curvature enhanced accelerator coverage [6–14], and the theory based on time-dependent transport [15, 16] are described. We then review the nucleation theory in terms of the continuum equations in Sect. 4.2.2. Diffusion-limited [17–22] and kinetically limited [23, 24] nucleation and growth are discussed. The fluid mechanical approach to copper electrodeposition is presented in Sect. 4.2.3 for the example of copper bump formation in microelectronics [25–32].

Since the size of recent LSI chips is as small as nanoscale, molecular simulations are important tools for microscopic analyses. The kinetic Monte Carlo (KMC) simulation is a promising technique with a wide range of applications. We discuss the KMC simulation and multiscale modeling in Sects. 4.3 and 4.4. The basic concept of the KMC method, the combination of the KMC method and continuum models, the multiscale modeling, and application to 3D device fabrication are presented [33–50]. Further developments of fast computing are discussed in Sect. 4.5 [51–56]. A summary and a brief comment on MD simulation [57, 58] are given in Sect. 4.6.

Since the purpose of the present article is to describe the mathematical frameworks and numerical methods, the parameter-setting in individual models is not stated although it is an important step in performing the simulations. We refer to the literature for setting parameters. Some details of the numerical algorithms which are important for simulation are summarized in Appendices.

Since this chapter is a review of more than 50 articles, some of the nomenclatures of variables and formulas are different from those in the original articles.

4.2 Mathematical Models for Copper Electrodeposition

The conventional mathematical models of electrodeposition are essentially boundary problems of the Laplace equation for current distribution and the diffusion equation for mass transport in solution. The deposition reactions and additive effects are incorporated in the boundary conditions. Since the electrode surface moves toward the solution as a result of electrodeposition, the technique to track the moving boundary is required for numerical calculations. In this section,

we overview the mathematical models for copper electrodeposition based on continuum models.

4.2.1 Mathematical Models for Superfilling

The success of the damascene process has accelerated the theoretical approach to copper electrodeposition. It has been shown experimentally that void-free filling of high-aspect ratio via holes and trenches can be obtained by the combination of suppressors (polyethylene glycol, PEG), halide ions (Cl^-), accelerators (bis 3-sulfopropyl disulfide, SPS), and levelers (Janus Green B, etc.). This section is concerned with an overview of recent theories to explain the additive effects, which are essential for superfilling within the framework of continuum models.

4.2.1.1 Diffusion-Consumption Model

The diffusion-consumption model is a traditional theory for leveling by suppressors [2, 3]. In this theory, the distribution of suppressors is assumed to be transport-limited, adsorbed on the surface where it inhibits metal deposition, and then consumed (annihilated from the surface). Figure 4.1a shows a schematic picture of the theory. Since the flux of suppressor comes from the solution far from the electrode, more suppressors are deposited around the opening of the hole than at the bottom. As a result, the metal deposition rate becomes higher at the bottom than at the top, resulting in bottom-up filling. Superfilling in the damascene process was first explained by this type of model [1, 4, 5]. The mathematical formulas used in the original paper of Andricacos et al. [1] are as follows:

The mass transport of metal ions and additives (suppressors) in the concentration boundary layer is assumed to occur only by diffusion. Assuming a stationary state, the concentrations of metal ions C, additives C_{ad} and the potential Φ obey the Laplace equations,

$$\nabla^2 C = 0, \nabla^2 C_{ad} = 0, \nabla^2 \Phi = 0, \tag{4.1}$$

C, C_{ad} and Φ are assumed to be independent in solution and are coupled only at the electrode surface. The boundary conditions at the electrode surface are

$$2FD\nabla C \cdot \mathbf{n} = \kappa_c \nabla \Phi \cdot \mathbf{n}, \tag{4.2}$$

$$C_{ad} = 0, \tag{4.3}$$

where F is Faraday's constant and κ_C is the electrical conductivity. $\mathbf{n}$ is the unit vector normal to the surface. Equation (4.2) arises from the balance of the current density and the flux of metal ions on the surface, where D is the diffusion constant

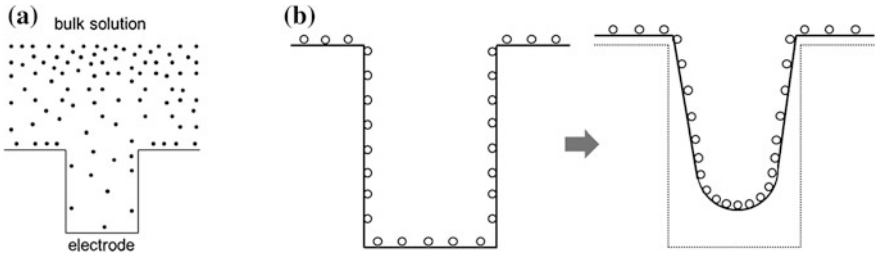

Fig. 4.1 **a** Image of the diffusion-consumption model. Suppressors (*solid circles*) diffuse from bulk solution to the electrode and annihilated. The concentration of suppressors is higher around the via top than at the bottom. **b** Image of the area change. Accelerators (*open circles*) are condensed as the bottom area is reduced

of metal ions. The condition (4.3) represents consumption of the additives on the surface. The current density at the electrode surface is given by the Tafel equation

$$i = i_0^{\infty}\psi\left(\frac{C}{C^{\infty}}\right)^{\gamma+\alpha/n} e^{\alpha F\Phi/RT}. \tag{4.4}$$

Here i_0^{∞} is the exchange current density of the additive-free bulk solution, ψ includes the suppressing effect of additives depending upon the spatial distribution of additive flux. α is a transfer coefficient and γ, n are constants. At the upper boundary in solution (the edge of the boundary layer), C and C_{ad} take the constant bulk values, C^{∞}, C_{ad}^{∞}, and $\nabla\Phi$ is calculated from the bulk current density. Equation (4.1) with the conditions Eqs.(4.2)–(4.4) has been solved using the moving boundary method [2]. The numerical simulations of this type of model showed that the diffusion-consumption theory can realize the bottom-up filling [1, 4, 5].

4.2.1.2 Curvature Enhanced Accelerator Coverage

The important characteristics of superfilling are (1) incubation period (conformal filling in the early stage), (2) bottom-up, and (3) overfilling and bump formation in the late stage. The diffusion-consumption theory can realize (2) bottom-up filling. However, it cannot explain the conditions (1) and (3). Also, in most of the experiments on superfilling, multiple additives (suppressor, accelerator, leveler) are required, while the diffusion-consumption model considers only suppressors. This means that an additional mechanism must be identified to explain the overall feature of superfilling.

A new theory has been proposed in terms of accelerators, which is known as the curvature enhanced accelerator coverage (CEAC) mechanism [6–8]. The key factor of this theory is the coverage of the accelerators on the electrode and the change in the surface area during the deposition process. Figure 4.1b is a

schematic picture of the idea of the CEAC mechanism. Assume that the accelerators are uniformly distributed on the feature surface. When the surface grows as a result of copper deposition, the surface of the bottom moves upward and the area becomes smaller. If the consumption of the accelerators is negligible, the surface coverage (concentration per unit area) of accelerators at the bottom increases. As a result, the deposition rate at the bottom becomes larger than that around the opening of the hole, which leads to bottom-up filling. A lot of papers have been published about the mathematical modeling and numerical simulations of the CEAC model. In the following, the basic formulas of the CEAC are summarized following the papers of Moffat et al. [6, 7, 9–14].

The system considered is copper electrodeposition with suppressors and accelerators. Assume that suppressors are quickly adsorbed on the surface and are soon replaced by the accelerators. Therefore, only the effect of accelerators is considered on the feature surface. The current density is assumed to be a function of the coverage θ_A of the accelerators and the overpotential η;

$$i = i(\theta_A, \eta). \tag{4.5}$$

Adsorbed accelerators float upon the growing metal surface, and their rate of consumption is assumed to be small. The time evolution of the coverage θ_A is represented by:

$$\frac{\partial \theta_A}{\partial t} = v\kappa\theta_A + R(\theta_A) + k_A\theta_A^q. \tag{4.6}$$

The local surface velocity v is given by $v = i\Omega/zF$, where Ω is the atomic volume and z is the valence of copper ions ($z = 2$ for Cu^{2+}). The reaction term $R(\theta_A)$ corresponds to the production rate of accelerants on the surface. The first term on the right-hand side of Eq. (4.6) represents the influence of the area change, where κ is the local curvature of the surface. This term means that the coverage θ_A depends on the sign of κ, i.e., θ_A will increase for the concave surface and decrease for the convex surface. Therefore, the growth rate of a concave surface becomes larger than that of flat or convex surfaces. The last term on the right-hand side of Eq. (4.6) shows the power law consumption of accelerants due to the incorporation. Equation (4.6) is solved with the equations representing the shape evolution of the electrode surface.

In the early works of Josell et al. [6], $k_A = 0$ and the following expressions were assumed,

$$i(\theta_A, \eta) = i_0(\theta_A)\left(1 - \frac{i}{i_L}\right)\exp\left(-\frac{\alpha(\theta_A)F}{RT}\eta\right), \tag{4.7}$$

$$R(\theta_A) = k^* C_A^i(1 - \theta_A), \tag{4.8}$$

where i_L is the transport-limited current density, C_A^i is the concentration of accelerators at the interface and k^* is the reaction rate. The exchange current density $i_0(\theta_A)$ and the transfer coefficient $\alpha(\theta_A)$ are obtained from independent

experiments on copper electrodeposition on a flat surface as a function of the accelerator coverageθ_A. The depletion of copper ions in solution was accounted for by the diffusion equation for copper ion density. The moving boundary has been treated by the level set method (LSM) [9].[1] Numerical calculations showed that the initial conformal deposition and bottom-up fill can be realized by this model depending upon the parameters. If the accelerators remain until the end of the filling, the accelerator concentration is large around the middle of the via, which leads to bump formation after filling is completed. Therefore, the CEAC is a model which reproduces the superfilling conditions.

The CEAC mechanism is regarded as a leveling theory in terms of the accelerators to control the roughness evolution of the surface [10]. The model has been modified to include the mass transport of accelerators in solution [9] and the surface diffusion of adsorbed accelerators [11]. It has also been extended to the multiple-additive system; PEG-SPS [12], PEG-SPS-Leveler [13, 14] to include the deactivation of accelerators by levelers. A summary of these works is found in Refs. [12, 14]. The idea of area change is quite general and has been incorporated in other mathematical forms as described in the following sections.

4.2.1.3 Time-dependent transport kinetics of additives

In the diffusion–consumption models in Refs. [1–5], a stationary state is assumed for the diffusion of suppressors. In the CEAC models cited in this section, time-dependent mass transport is taken into account for copper ions and accelerators, but not for suppressors. Akolkar and Landau pointed out that different mechanisms appear in the early stage and the late stage of the filling process due to the time-dependent transport and interactions between additives [15, 16]. They observed in their experiments [15] that PEG adsorbs on the copper surface almost instantaneously, while the diffusion of the PEG in solution is slow. SPS, on the other hand, diffuses rapidly in solution and adsorbs on copper surface moderately fast. The replacement of the adsorbed PEG by SPS is rather slow compared to the adsorption of PEG and SPS on the additive-free surface.

Taking into account these differences in the time scales, Akolkar and Landau developed a one-dimensional transport–adsorption model [16]. For a high-aspect ratio via (the radius R_V and the depth L_V), the radial variation of concentration is negligible and the time and space variation of the PEG concentration C_I in the axial direction (z-direction) parallel to the via sidewall is considered. The mass balance in the via hole leads to the following diffusion–reaction equation for C_I.

$$\frac{\partial C_I}{\partial t} = D_I \frac{\partial^2 C_I}{\partial z^2} - \frac{2}{R_V}\left[k_I C_I(1-\theta_I-\theta_A) - kC_A^b\theta_A\right] \tag{4.9}$$

[1] LSM is a feasible method to track the moving boundary. The formulas are given in Appendix A.

The first term on the right-hand side is the diffusion term, where D_I is the PEG diffusion constant. The second term represents the reactions on the surface, where k_I is the adsorption rate constant, and θ_I and θ_A are the surface coverages of PEG and SPS, respectively. The second term in the square brackets represents the displacement of PEG by SPS, where k is the reaction rate. The concentration of SPS in the via is assumed to be the same as the bulk value C_A^b due to the rapid diffusion.

The time variations of the coverages θ_I and θ_A are represented by the balance of the reactions as

$$\frac{\partial \theta_I}{\partial t} = \frac{1}{\Gamma_I}\left[k_I C_I(1-\theta_I-\theta_A) - kC_A^b\theta_A\right] \tag{4.10}$$

$$\frac{\partial \theta_A}{\partial t} = \frac{1}{\Gamma_A}kC_A^b(1-\theta_I-\theta_A) + \frac{1}{\Gamma_I}kC_A^b\theta_I \tag{4.11}$$

The difference in the molecular size of PEG and SPS is taken into account by Γ_I and Γ_A, where $\Gamma_A/\Gamma_I \cong 13.33$. Equation (4.10) indicates that the coverage of PEG increases rapidly (first term) and is slowly replaced by SPS (second term). At the via bottom, however, PEG deposition is hindered by slow diffusion. The first and second terms on the right-hand side of Eq. (4.11) show the rapid adsorption of PEG on additive-free surface and the slow displacement of PEG, respectively. The total current density arises from the sum of the current densities of PEG-covered area, SPS-covered area, and additive-free copper surface, which are represented by

$$\begin{aligned} i_{tot} = {} & i_{0,I}\theta_I \exp\left(\frac{\alpha_I F\eta}{RT}\right) + i_{0,A}\theta_A \exp\left(\frac{\alpha_A F\eta}{RT}\right) \\ & + i_{0,Cu}(1-\theta_I-\theta_A)\exp\left(\frac{\alpha F\eta}{RT}\right), \end{aligned} \tag{4.12}$$

where $i_{0,I}, i_{0,A}, i_{0,Cu}$ are exchange current densities and $\alpha_I, \alpha_A, \alpha$ are transfer coefficients corresponding to the three areas mentioned above. Equations (4.9–4.12) constitute the coupled equations for the transport–deposition process of PEG-SPS system.

The area reduction in the late stage, especially at the via bottom, is incorporated in the model in the form

$$\theta_A^{new}(t) = \left(\frac{A_{init}}{A(t)}\right)\theta_A^{TA}(t), \tag{4.13}$$

where $\theta_A^{TA}(t)$ is the time and area dependent surface coverage of SPS, and A_{init} and $A(t)$ are the initial area and the area at time t, respectively. The above equations are solved numerically using the moving boundary method.

Figures 4.2 and 4.3 show the time variations of surface coverage θ_I and θ_A at the via bottom ($z = L_V$) and via top ($z = 0$) produced by the simulation of the filling process (L_V/R_V = 5). Two distinct time regions are clearly observed.

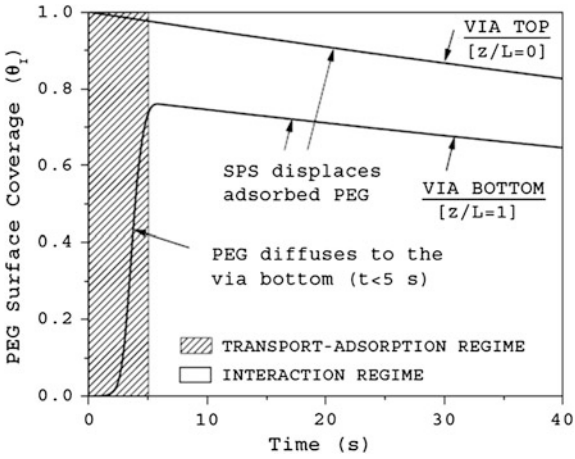

Fig. 4.2 The time-dependent PEG surface coverage at the via top and at the via bottom. The cross-hatched region ($t < 5$ [s]) is the transport-adsorption regime and unmarked ($t > 5$ [s]) is the interaction regime. The *upper line* shows the via *top* and the *lower line* via *bottom*. The kinetics parameters are listed in Table 4.1 in Ref. [16]. (Reproduced from Fig. 4.5 of Ref. [16] by the permission of The Electrochemical Society)

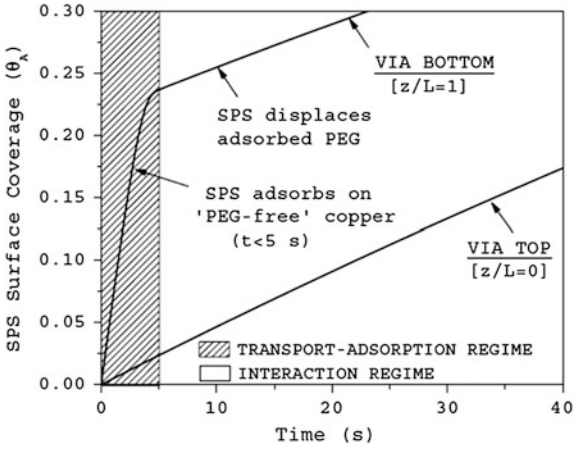

Fig. 4.3 The time-dependent SPS surface coverage at the via top and at the via bottom. The cross-hatched region ($t < 5$ [s]) is the transport-adsorption regime and unmarked ($t > 5$ [s]) is the interaction regime. The *upper line* shows the via *bottom* and the *lower line* via *top*. The kinetics parameters are listed in Table 4.1 in Ref. [16]. (Reproduced from Fig. 4.6 of Ref. [16] by the permission of The Electrochemical Society)

At $t = 0 \sim 5$ [s] the transport of additives is important, i.e., PEG adsorbs around the via top rapidly, while the via bottom is not covered with PEG due to the slow diffusion. The via bottom is covered with SPS which is expected to initiate the initial bottom-up fill. At $t \gtrsim 5$ [s], the interaction between additives becomes dominant and SPS displaces the PEG on the sidewall. The growth of the via bottom is even more accelerated by the effect of area reduction Eq. (4.13), which results in the bottom-up filling as shown in Fig. 4.4. The details of the simulation are described in Ref. [16].

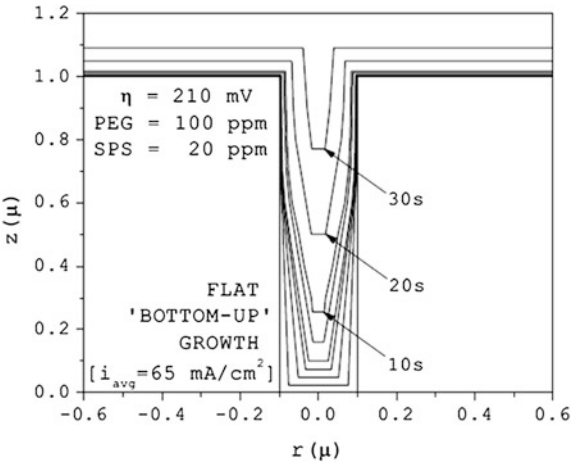

Fig. 4.4 Deposit growth simulation during bottom-up fill in a via with $R = 0.1[\mu m]$ and $L = 1[\mu m]$ at an overpotential of 120 [mV] in the presence of 20 [ppm] SPS and 100 [ppm] PEG. The kinetics parameters are listed in Table 4.1 in Ref. [16]. (Reproduced from Fig. 4.8 of Ref. [16] by the permission of The Electrochemical Society)

4.2.2 Continuum Models for Nucleation and Growth

Continuum models have been applied not only to macroscopic shape evolution but also to microscopic nucleation process. In dual damascene technology, direct electrodeposition of copper on barrier layers other than copper (e.g., ruthenium or titanium) has attracted attention to circumvent the limitations of plating copper seed layer on submicron vias and trenches. The key issue is to control the nucleation density in the early stage of electrodeposition to plate a continuous copper film which will lead to void-free filling. There has been a lot of work on nucleation and growth in copper electrodeposition on foreign substrates. Following is an overview of two models for nucleation and growth in different regimes.

4.2.2.1 Diffusion-Limited Growth

A simulation model for nucleation and growth under diffusion control has been developed by West et al. [17–19]. They considered the growth of hemispherical nuclei on a foreign substrate. The main focus is on mass transport in solution. The time dependence of the number of nuclei on the surface, $N(t)$, is

$$\frac{dN}{dt} = k_n \left(\frac{C}{C^{\infty}} \right)^n (N_0 - N) \tag{4.14}$$

where k_n is the nucleation rate constant, C and C^{∞} are the concentration of metal ions and that of the bulk, respectively. For instantaneous nucleation $N(t)$ is equal to the number of nucleation sites N_0. Once the number of nuclei is determined, nuclei are added to the surface stochastically by the MC method.

Nucleation is followed by the growth of nuclei. The concentration is governed by the diffusion equation

$$\frac{\partial C}{\partial t} = D\nabla^2 C \tag{4.15}$$

with the initial and boundary conditions

$$C = C^{\infty} \text{ at } t = 0 \tag{4.16}$$

$$C = C^{\infty} \text{ far from the electrode} \tag{4.17}$$

On the electrode surface, copper deposition occurs on the surface of the copper nuclei, but not on the foreign substrate. The flux normal to the surface is:

$$f = -D\frac{dC}{dn} = 0 \text{ at non-nucleated site} \tag{4.18}$$

$$f = -D\frac{dC}{dn} = k_G C, r = r_m(t) \text{ at a nucleus} \tag{4.19}$$

where k_{G} is the deposition rate constant. The growth is diffusion-limited when $C \to 0$ and $k_{\mathrm{G}} \to \infty$. $r_{\mathrm{m}}(t)$ is the radius of the nucleated hemispherical particle evaluated from the mass balance equation

$$\frac{dr_{\mathrm{m}}}{dt} = V_{\mathrm{M}} f \tag{4.20}$$

V_{M} is the molar volume of deposited species. These equations are coupled with the current density

$$i(t) = nFN(t)\left[f(t)2\pi r^2(t)\right]_{\mathrm{avg}} \tag{4.21}$$

$[\,]_{\mathrm{avg}}$ is the average over the existing nuclei. West et al. studied diffusion-limited growth ($k_{\mathrm{G}} = 0$) [17], deviation from the diffusion control due to $k_{\mathrm{G}} > 0$ [18] and the dependence of $N(t)$ on the concentration C [19]. Emekli and West [20–22] extended the theory to include additives and studied the influence of suppressors on nucleation using the same model.

4.2.2.2 Kinetically Limited Growth

Under the condition where the concentration of copper ions near the electrode can be assumed to be constant ($C = C^{\infty}$), nucleation and growth become kinetically limited. In this regime, the basic processes are the reduction of copper ions, surface diffusion of adatoms, and crystallization (nucleation and incorporation of adatoms into nuclei). The crucial point in the modeling is the accurate treatment of surface diffusion, which is much faster than the other surface processes. Stephens and

Alkire applied the "island dynamics" method to study the nucleation of copper with additives onto foreign substrates [23, 24].

The key variable in the theory is the adatom density $c_{\mathrm{ad}}(x, y)$ on the electrode surface ((x, y)-plane). The nucleation rate is given by the average adatom density

$$\frac{dN}{dt} = D_{\mathrm{s}}\sigma\langle c_{\mathrm{ad}}(x, y)\rangle, \tag{4.22}$$

where D_{s} is the surface diffusion constant of adatoms and σ is the reaction rate constant. The growth of the nuclei occurs when adatoms are incorporated into the island edge after surface diffusion. The edge velocity of a nucleus is evaluated by:

$$v(x, y) = D_{\mathrm{s}}(x, y)A_{\mathrm{m}}[\mathbf{n} \cdot \nabla c_{\mathrm{ad}}(x, y)|_{\mathrm{inside}} - \mathbf{n} \cdot \nabla c_{\mathrm{ad}}(x, y)|_{\mathrm{outside}}] \tag{4.23}$$

In Eq. (4.23), "inside" refers to the attachment of an adatom to the edge boundary from the top of the island (i.e., incorporation of an adatom deposited on the island) and "outside" refers to the attachment of an adatom from the lateral plane outside the island. The velocity $v(x, y)$ is used to track the moving boundary of the island by the LSM ((A.1) in Appendix A). When additives are deposited on the surface, they block the surface diffusion and the available area for adatom diffusion is less than the total area of the electrode surface. This is taken into account by defining the effective surface diffusion constant which is proportional to the fraction of available sites $\theta_{\text{available site}}$ as

$$D_{\mathrm{effective}}(x, y) = \theta_{\mathrm{availablesite}} D_{\mathrm{s}}(x, y) \tag{4.24}$$

Using this approximation, the concentration field of adatoms $c_{\mathrm{ad}}(x, y)$ is simulated by the extended diffusion equation

$$\frac{\partial c_{\mathrm{ad}}(x, y)}{\partial t} - D_{\mathrm{effective}}(x, y)\nabla^2 c_{\mathrm{ad}}(x, y) = F \tag{4.25}$$

where F is the flux of adatoms onto the surface. Stephens et al. [23, 24] studied the influence of multiple additives (PEG, SPS) on the nucleation and growth process of copper on Cu and Au using the reaction models, which are the same as those used in the KMC simulations [38–40].

4.2.3 Fluid Mechanical Approach

In damascene electroplating and the nucleation problem presented in the previous sections, the effect of convection is not included in the modeling. The main driving force for mass transport is diffusion. When the feature size becomes $10 \sim 100\mu$m or larger, on the other hand, the fluid mechanical flow and vortex formation will play an important role in the electrodeposition process. The flow patterns around the electrode with cavities have been widely studied by numerical simulations. The role of mass transport in etching of rectangular cavities has been studied by many

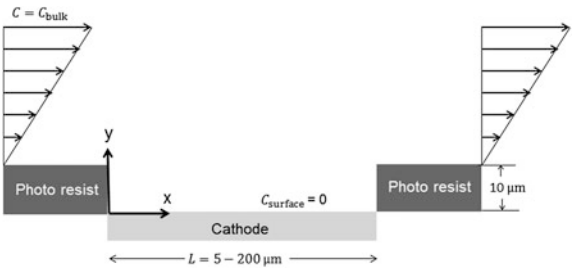

Fig. 4.5 Illustration of two-dimensional cross section of photoresist and cathode. (Width : L, height : h)

authors using the numerical fluid dynamics computations. Alkire et al. developed two-dimensional numerical fluid dynamics computation to study the etching of copper [25–27]. Shin and Economou studied electrolytic etching at a moving boundary for forced and natural convection [28].

The influence of fluid mechanical flow on the shape evolution of electrodeposited copper bumps has been studied by Kondo et al. using numerical fluid dynamics computation [29–32]. Electrodeposited bumps are important microconnectors for high density interconnection between microprocessors, random access memories, the connection between liquid crystal display and driver chips, and so on. The bumps are electrodeposited on a dot-shaped cathode $10 \sim 200\mu$m in diameter. Kondo et al. showed that the influence of macroscopic flow and vortex formation is important for the control of electrodeposited bump shape and uniformity in height [29, 30].

The key parameter in the theory is the Peclet number P_e which represents the ratio of the flow speed to that of diffusion. Figure 4.5 illustrates the model system of two-dimensional cross section of photoresist and cathode with the boundary conditions. The Peclet number for this system is

$$P_e = \frac{hu_{y=2h}}{D}, \tag{4.26}$$

where h is the height of the resist, u is the flow velocity and D is the diffusion constant. The basic equations are the equation of continuity, Navier–Stokes equations and mass transfer equation

$$\frac{\partial u}{\partial x} + \frac{\partial u}{\partial y} = 0 \tag{4.27}$$

$$\rho\left(u\frac{\partial u}{\partial x} + v\frac{\partial u}{\partial y}\right) = -\frac{\partial P}{\partial x} + \mu\left(\frac{\partial^2 u}{\partial x^2} + \frac{\partial^2 u}{\partial y^2}\right) \tag{4.28}$$

$$\rho\left(u\frac{\partial v}{\partial x} + v\frac{\partial v}{\partial y}\right) = -\frac{\partial P}{\partial x} + \mu\left(\frac{\partial^2 v}{\partial x^2} + \frac{\partial^2 v}{\partial y^2}\right) \tag{4.29}$$

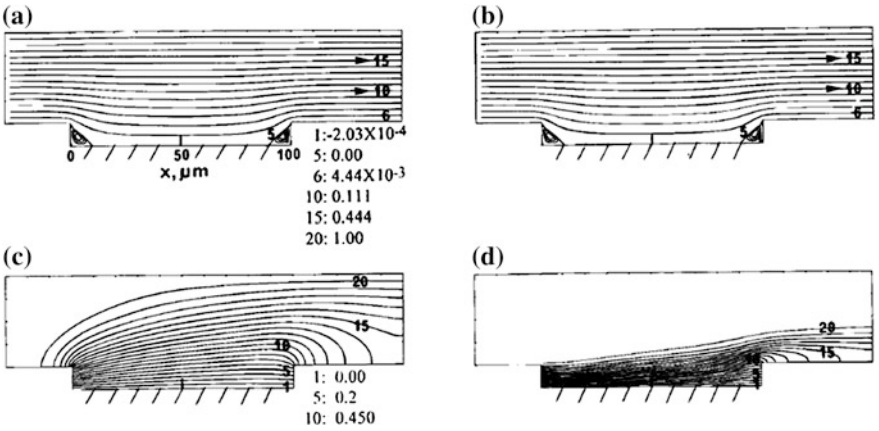

Fig. 4.6 Effects of Peclet numbers on streamlines and isoconcentration contours. The cavity width is100[μm]. Streamlines for $P_e = 1.31$ (**a**) and 41.6 (**c**). Isoconcentration contours for $P_e = 1.31$ (**b**) and 41.6 (**d**). (Reproduced from Fig. 4.4 of Ref. [29] by the permission of The Electrochemical Society)

$$u\frac{\partial C}{\partial x} + v\frac{\partial C}{\partial y} = D\left(\frac{\partial^2 C}{\partial x^2} + \frac{\partial^2 C}{\partial y^2}\right) \tag{4.30}$$

where ρ, P, μ and C are the density, static pressure, viscosity, and the concentration, respectively.

Figure 4.6 shows examples of the normalized stream functions and isoconcentration contours for $P_e = 1.31$(a,c) and 41.6 (b,d). The solution flow is from left to right and the streamline labeled 6 is the penetration flow. Vortices are observed at the corners both at up and downstream sides. In the isoconcentration contours the difference in the thickness of the concentration boundary layers is observed for $P_e = 1.31$ and 41.6. The local copper deposition rate on the cathode depends on the dimensionless Sherwood number,

$$Sh = \frac{L}{\Delta C}\left(\frac{\mathrm{d}C}{\mathrm{d}y}\right)_{y=0} \tag{4.31}$$

which shows the ionic transport due to the concentration gradient.(Fig. 4.7) Sh shows the maximum at $x = 0\mu$m for $P_e = 1.3$, gradually decreases toward the downstream side and slightly increases at $x \gtrsim 90\mu$m. The maximum height at around $x = 0\mu$m is due to the vortex which captures copper ions and enhances the local mass transport to the cathode. The vortex at the downstream side also enhances the local mass transport of copper to the cathode, which leads to a slight increase in Sh. For $P_e = 41.6$, on the other hand, mass transport is mainly controlled by convection due to the penetrating flow and vortex rather than diffusion. The vortex on the upstream side does not provide ions to the cathode and local

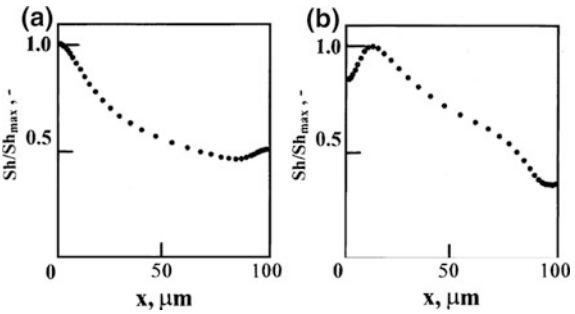

Fig. 4.7 Effects on Peclet numbers on flux (normalized Sherwood number). P_e = 1.31 (**a**) and 41.6 (**b**). (Reproduced from Fig. 4.5 of Ref. [29] by the permission of The Electrochemical Society)

resistance arises. This leads to a slight shift of the maximum flux to $x \cong 10\mu$m. These flux profiles coincide with the bump shape observed in experiments as shown in Ref. [29]. Kondo et al. also studied the flow patterns for higher Peclet numbers [31] and the current distribution on copper bumps with photoresist sidewall angle by numerical simulation and experiments [32]. These works show that the interplay between the convection and diffusion is the key factor for control of bump formation.

4.3 Kinetic Monte Carlo Simulation and Multiscale Modeling

In the previous section, the recent theories based on continuum models have been presented. This and the following sections are devoted to molecular simulations of copper electrodeposition, in which ions and additive molecules are treated as particles. The KMC simulation is a stochastic method to simulate the time evolution of many-particle systems using rate constants and random numbers [33]. Since the KMC method is based on statistical mechanics and the mathematical theory of stochastic process, it has a wide range of application. In electrochemistry, the KMC method has been used as a feasible tool for simulations taking into account the microscopic process of nucleation and growth.

One of the characteristics of electrodeposition which makes the molecular simulation approach difficult is the multiscale aspect in time and space. For example, the microscopic surface reactions (of the order of nanometer and nanosecond) are dependent upon the concentrations of ions which are controlled by the macroscopic mass transport in the diffusion layer (micrometer and millisecond or larger scales). Since the KMC method is essentially an atomic-scale method, it has been extended to combination with some tools which deal with large-scale and long-time quantities in the application to electrochemical systems. Therefore, a hybridized method of KMC and continuum models have been developed for the unified simulation from micro to macro scales. In this section, we first describe the basic concept and modeling of the KMC simulation for crystal

growth, and then the recent sophistications of the multiscale KMC-continuum simulation for copper electrodeposition are reviewed referring to the works of Alkire et al. [34–40].

4.3.1 Solid-on-Solid Model

Solid-on-Solid (SOS) model is a basic model for crystal growth, which is widely used in theoretical and numerical studies [41, 42]. The system is a square (2D) or a cubic (3D) lattice as shown in Fig. 4.8. Each lattice site represents a solid atom, a liquid atom, or a vacancy. (In a coarse-grained system a site represents a group of atoms.) We first consider the additive-free case and assume three events such as adsorption, desorption, and surface diffusion to change the state of the sites. The rate constants are defined for these three events such as adsorption rate k_n^+, desorption rate k_n and surface diffusion rate k_{nm}. The suffix n represents the characteristics of the site on which the event occurs. (e.g., the number of nearest neighbor atoms) In k_{nm}, n and m represent the information before and after the movement, respectively. These rates are the functions of the binding energy, activation energy for surface diffusion, ionic concentration, and so on. The definitions of these rate constants characterize the model.

In the SOS model, adsorption occurs only "on" the surface sites, i.e., at the nearest neighbor vacant sites in the y-direction (Fig. 4.8). As a result, vacancy formation is inhibited in the SOS model. Also, overhang and shadowing are not allowed to occur during the growth. Therefore, the SOS model is appropriate for describing layer-by-layer growth, but is not suitable for rough surface and dendrites.

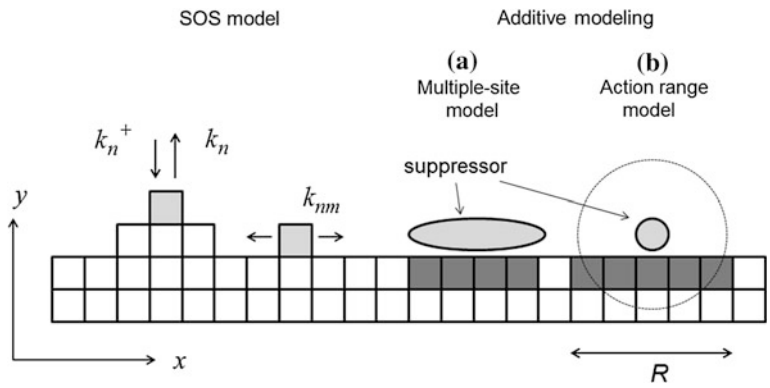

Fig. 4.8 *Left* Schematic picture of the SOS model. *Squares* denote solid atoms and *gray squares* are adatoms. *Right* Two types of additive modeling. **a** Multiple-site model and **b** Action range model. (*R*: action range)

Additives are incorporated in the SOS model as follows. Additives occupy lattice sites in the same way as metal atoms, and the adsorption and desorption rates of additives are given as input parameters. The adsorbed additives have suppressing or accelerating effects on metal deposition at the surrounding sites. In the case of polymer suppressors (such as PEG in copper electrodeposition), the molecular volume is much larger than that of metal atoms. There are two methods to take into account the size difference. One way is to assume that an additive occupies more than one lattice site and deposition of metal atoms on the sites covered by the additive is inhibited (multisite model) as illustrated in Fig. 4.8a [38]. An alternative method is shown in Fig. 4.8b. The additive occupies one lattice site and an action range R is defined around it. Metal deposition on the sites within the action range is inhibited. The range R is chosen to reflect the effective size of the polymer (e.g., Flory radius of a polymer chain). The latter model can be applied to the accelerators, i.e., the deposition rate of copper within the action range is assumed to be larger than that on the sites outside the action range.

In the KMC simulation, the state of each site is changed sequentially by using random numbers. There are two types of algorithm for KMC simulations. The simple algorithm is the rejection method. The procedure is to choose a site and an event randomly and decide if the event is realized or not by using random numbers. Although the coding of the rejection method is simple, it is not efficient in a situation where a lot of rejections are selected. The second type of algorithm is a rejection-free algorithm which was proposed for the simulation of Ising spin systems by Boltz et al. (BKL method) [43]. The general form for this type of algorithm is given by Gillespie [44]. The procedure is to tabulate the candidate atoms (or sites) and the reaction rates, decide the events using the rates and the random numbers, and renew the table after the event.[2] This method is efficient because rejection does not occur in the sequence. The point for the efficiency of the rejection method is how to reduce the number of rejections. The efficiency of the rejection-free method depends on the algorithm used to search and revise the tables. A comparison of the efficiencies of these methods is given in Ref. [33].

4.3.2 KMC-Continuum Combination

The rate constants k_n^+, k_n and k_{nm} depend not only on the physical quantities which can be assumed to be constant (such as the binding energy) but also on the quantities which change during the deposition (such as the ionic concentration in solution). Therefore, in most applications, the SOS model is combined with the continuum models which represent the time dependence of the quantities in the solution. The program consists of the KMC code and the continuum code [34]. The continuum code calculates the quantities in solution (concentration, potential, etc.)

[2] The BKL algorithm for crystal growth is given in Appendix B.

by solving the partial differential equations. It gives the information necessary for determining the rate constants for the KMC code. The KMC code simulates the crystal growth using the rate constants and gives the renewed surface information (the change in the concentration and the surface structure) back to the continuum code. The continuum code simulates the solution quantities using the renewed information as the boundary conditions. Since the surface moves into the solution as a result of crystal growth, the numerical treatment of moving boundaries is required.

The combination of the KMC method and continuum models is a general framework of the microscopic simulation of electrodeposition. Pricer et al. combined the (2 + 1)D SOS model with 1D diffusion equation for copper ions to simulate the surface morphology in copper electrodeposition [35]. Here (2 + 1)D means the two-dimensional substrate surface (2) and one layer of deposited atoms (+1). Drews et al. studied the effect of additives (PEG, Cl^-, MPSA) on the surface morphology [36]. Drews et al. extended the SOS model to represent the fcc (111) surface and studied the nucleation process by using the KMC simulation [37].

4.3.3 Multiscale KMC-Continuum Hybrid Simulation for Trench Filling

An extensive multiscale KMC-continuum simulation of trench filling by copper electrodeposition has been developed by Alkire et al. [38–40]. In their model, four kinds of additives (PEG, SPS, Cl^-, 1-2-hydroxyethyl-2-imidazolidinethione (HIT)), 14 surface reactions, and three homogeneous reactions in solution are taken into account. The system consists of three parts; (1) mass transport and reactions in solution, (2) surface shape evolution, and (3) crystal growth on the surface. Mass transport in solution is represented by the mass balance equation

$$\frac{\partial C_i}{\partial t} = D_i \nabla^2 C_i + z_i F u_i \nabla \cdot (C_i \nabla \Phi) + A_i, \tag{4.32}$$

where D_i, C_i, z_i and u_i are the diffusion constant, the concentration, the valence, and the mobility of species i, respectively. Φ is the potential and A_i is the production rate of species i due to the homogeneous reaction in solution. Equation (4.32) represents the overall material conservation in solution. The flux of species i is given by

$$\mathbf{N}_i = D_i \nabla C_i + z_i F u_i C_i \nabla \Phi. \tag{4.33}$$

The boundary conditions on the top bulk boundary are the bulk values

$$C_i = C_i^{\infty}, \Phi = \Phi^{\infty}. \tag{4.34}$$

The boundary conditions on the nonactive boundary and the active boundary (electrode surface) are:

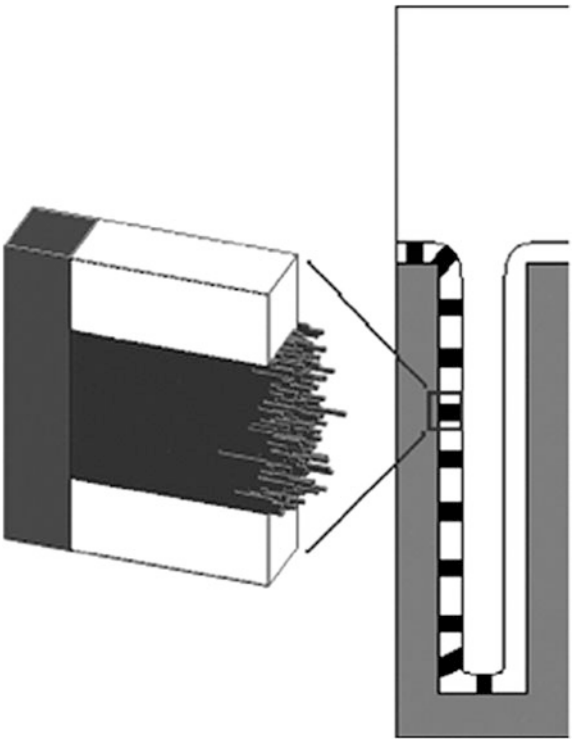

Fig. 4.9 The relation between the KMC code and the continuum code. *Right* Ten individual KMC domains along the wall of a trench. *Left* The enlarged image is one of the KMC domains. (Reproduced from Fig. 4.3 of Ref. [38] by the permission of The Electrochemical Society)

$$\mathbf{N}_i \cdot \mathbf{n} = 0, \tag{4.35}$$

$$\mathbf{N}_i \cdot \mathbf{n} = J_i, \tag{4.36}$$

respectively, where J_i is the flux of species i computed by the KMC code. These equations are solved by the finite volume (FV) method using the data from the KMC code as the boundary conditions.

The shape evolution of the growing trench surface as a result of the deposition reactions is tracked by LSM (Appendix A). The FV code and the LSM code are coupled to form the moving boundary which is also coupled with the KMC code. The relation between the KMC code and the moving boundary is illustrated in Fig. 4.9. There are 10 KMC simulation domains along the surface. In these domains, the crystal growth is simulated by the KMC code of the SOS model. The result of the KMC simulation in each domain is passed to the computation of the moving boundary. The results of the LSM code and the FV code are reflected in turn in the KMC code.

The reactions included in the model are summarized in Table 4.1. The copper ions are reduced in two steps, $Cu^{2+} + e^- \rightarrow Cu^+$, $Cu^+ + e^- \rightarrow Cu$. Four kinds of additives are included; PEG, SPS, Cl^-, and HIT. Chloride ions are combined with Cu^+ to produce CuCl on the surface (reaction 5). PEG is adsorbed on the surface as

Table 4.1 Species and chemical reactions in copper electrodeposition used in the simulations [38–40, 49, 50]

Reaction no.	Species and reactions
	Surface reactions
1	$Cu^{2+} + e^- \rightarrow Cu^+$
2	$Cu^+ + e^- \rightarrow Cu$
3	$Cu \rightarrow Cu^+ + e^-$
4	$Cu \rightarrow Cu(\text{surface diffusion})$
5	$Cu^+ + Cl^- \rightarrow CuCl$
6	$CuCl \rightarrow Cu^+ + Cl^-$
7	$CuCl + e^- \rightarrow Cu + Cl^-$
8	$CuCl + PEG \rightarrow CuClPEG$
9	$CuClPEG \rightarrow CuCl + PEG$
10	$SPS + 2e^- + 2H^+ \rightarrow 2MPS$
11	$Cu^+ + MPS \rightarrow Cu(I)thiolate + H^+$
12	$Cu(I)thiolate + H^+ \rightarrow Cu^+ + MPS$
13	$Cu^+ + Cu(I)thiolate + e^- \rightarrow Cu(I)thiolate + Cu$
14	$Cu(I)thiolate + HIT \rightarrow Cu(I)HIT + MPS$
15	$Cu(I)HIT + H^+ + Cu(I) \rightarrow HIT + Cu_2$
	Homogeneous reactions in solution
16	$MPS \leftrightarrow H^+ + thiolate^-$
17	$H_2SO_4 \leftrightarrow HSO_4^- + H^+$
18	$HSO_4^- \leftrightarrow SO_4^{2-} + H^+$

CuClPEG (reaction 8). The suppressing effect of CuClPEG is expressed by the multiple-site model (Fig. 4.8a). SPS produces two MPS molecules which create Cu(I)thiolate (reactions 10, 11, and 16). Cu(I)thiolate has a catalytic effect on the reduction of Cu^+ to Cu (reaction 13). The leveler HIT deactivates the Cu(I)thiolate (reaction 14) and lowers the copper deposition rate.

In the KMC code, one lattice site is assumed to represent a mesoparticle which contains a group of particles. This is to track a larger scale shape evolution. The area change is calculated from the local curvature by the LSM code and sent to the KMC codes at the different trench surface location. The KMC code calculates the changes of the surface coverage of Cu(I)thiolate at different locations. The concentrations of the Cu(I)thiolate are corrected by inserting additional Cu(I)thiolate so that the total mass of the chemical species is conserved.

Figure 4.10 shows the results of the simulation corresponding to the experimental condition; 0.3 M $CuSO_4$, 125 g/L H_2SO_4, 0.3 g/L PEG, 50 ppm Cl^- and 10 ppm SPS. The trench is 0.2 μm wide and is 1 μm high. The rate constants for the reactions in Table 4.1 are given in Refs. [38, 39]. Figure 4.10a shows the shape evolution pattern, b shows the time and space dependences of the surface coverage of Cu, CuCl, CuClPEG, and Cu(I)thiolate. In each figure, the position "0" corresponds to the trench opening and "0.5" is the center of the trench. Figure 4.10c shows the time and space dependencies of the reaction rates of reactions 2, 7, and 13 evaluated in the simulation. Figure 4.10a clearly shows the characteristics of superfilling; (i) initial incubation period, (ii) bottom-up, and (iii) overfill after the

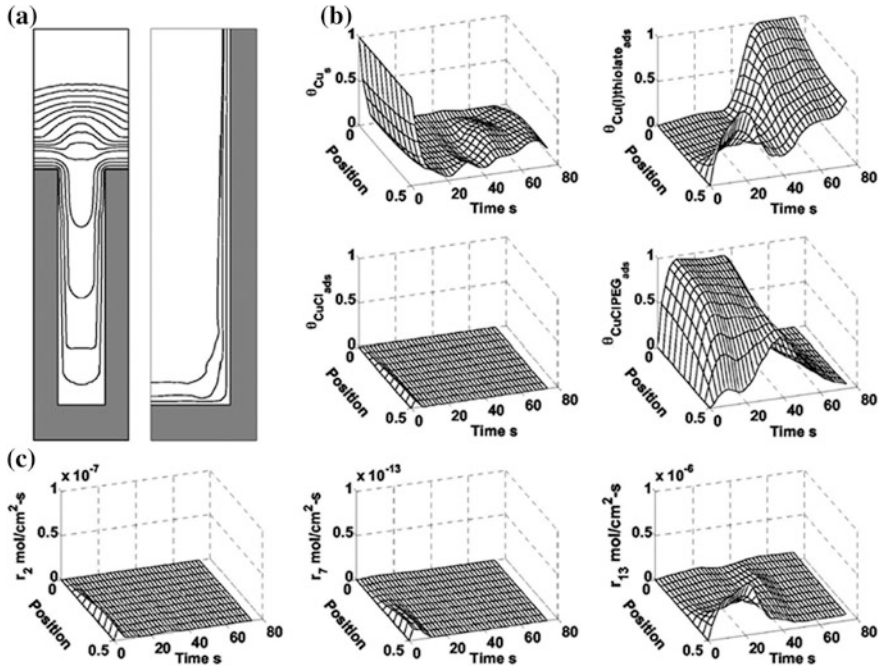

Fig. 4.10 Simulation of trench filling. **a** Two trench cross-sections showing the shape evolution. *Left* every 5 s for 0–70 s and *right* every 1 s for 0–3 s. **b** The surface coverage versus time and position for four surface species during the trench infill. **c** The time-dependent reaction rate distribution for the three reactions associated with copper electrodeposition (reactions 2, 7, and 13). The positions 0 and 0.5 correspond to the trench opening and the center of the trench, respectively. (Reproduced from Fig. 4.1 of Ref. [40] by the permission of The Electrochemical Society)

filling. Figures 4.10b, c shows that CuClPEG is distributed in the upper half of the trench and Cu(I)thiolate in the lower half of the trench. From the spatial distribution of r_{13} (the rate of reaction 13), the bottom-up fill is mainly due to the accelerating effect of Cu(I)thiolate. These results show that the combination of the KMC code, LSM code, and the FV code can perform the overall simulation of trench filling taking into account the slow mass transport represented by the mass balance equation (4.9) and the microscopic reactions listed in Table 4.1.

4.4 Solid-by-Solid Model and 3D Shape Evolution

The SOS model represents an ideal situation in which a new atom is deposited on a surface solid atom only in the vertical direction, and no vacancy is formed in the deposited films. In real deposition, lattice defects such as vacancies and

dislocations, which are created during electrodeposition, play an important role in determining the physical properties of the film. The SOS approach has been extended to a model, which includes void formation by Kaneko et al. [45, 46]. The new model is called the Solid-by-Solid (SBS) model. This section is concerned with the basic properties of the SBS model and its application to the 3D shape evolution of via and trench fillings.

4.4.1 Solid-by-Solid Model

We consider a 2D square lattice each site of which is occupied by either a liquid atom or a solid atom, otherwise vacant. The schematic picture of the model is shown in Fig. 4.11. Growth is in the *y*-direction and a periodic boundary condition is used in the *x*-direction. Surface solid atoms are denoted by bright gray squares which are distinguished from the solid atoms embedded in the film (dark gray squares). Empty sites surrounded by solid atoms with no contact with the liquid are defined as vacancies. Three events are assumed to occur to change the state of each site: adsorption, desorption, and surface diffusion. As for adsorption, the SOS criterion is removed, that is, a new atom is deposited on any nearest neighbor sites of the surface solid atom (as indicated by the arrows in Fig. 4.11). In order to allow this deposition, the surface solid atoms must be defined even when the surface has a rough structure. An accurate algorithm to search the surface solid atoms is a key factor for extension of the SOS model to the SBS model. The searching algorithm is given in Appendix C.

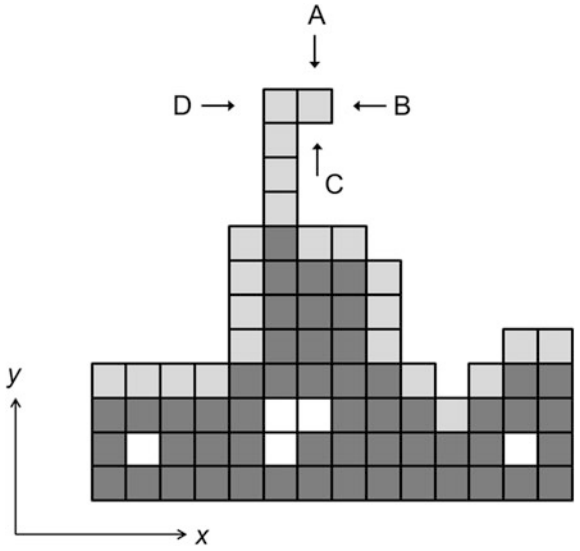

Fig. 4.11 Illustration of the SBS model. *Dark gray squares* are solid atoms and *bright gray squares* are surface solid atoms. *White squares* are vacancies. The adsorption of new atoms occurs from any directions indicated by *arrows* A, B, C, D

The rate constants for adsorption k_n^+, desorption k_n and surface diffusion k_{nm} are assumed to have the following relations; [41, 42]

$$\frac{k_n}{k_n^+} = \exp\left[(n_k - n)\frac{\varphi}{k_B T} - \frac{\mu}{k_B T}\right], \tag{4.37}$$

$$k_{nm} = \frac{k_n k_m^+}{k_1^+}\exp\left[\frac{\varphi - E_d}{k_B T}\right], \tag{4.38}$$

where φ is the binding energy between solid atoms, μ is the electrochemical potential and E_d is the activation energy for the surface diffusion. n_k is the number of bonds at a kink site. ($n_k = 2$ for 2D lattice and 3 for 3D lattice) k_B is Boltzmann constant and T is the temperature. The relation (4.37) is derived from the microscopic detailed balance at a kink site [42]. This model is called the SBS basic model hereafter.

The advantage of the SBS model is that one can perform the simulation of crystal growth on complex nonflat surfaces which accompanies void formation. The shape evolution can be simulated without using any additional algorithm to track the moving boundary. Therefore, it is suitable for the simulation of filling small features such as damascene electroplating. The effects of suppressors, accelerators, and levelers have been studied by the KMC simulations of 2D SBS model and the condition for void-free filling has been discussed. [47, 48]

It is straightforward to extend the SBS model to a 3D system. Figure 4.12 shows the simulation of dual damascene using the 3D SBS basic model without additives. The initial surface has a trench with a cylindrical via hole at the bottom. The aspect ratio of the trench and the via is unity. Periodic boundary conditions are used in the lateral directions. It is observed that the via hole is first filled with deposited atoms forming voids in the hole. Then the trench is filled forming seams which are elongated in the growth direction in the middle of the trench. Since ionic transport is not included in the SBS basic model, the filling is almost conformal. The surface is clearly defined at every KMC step by the searching algorithm given in Appendix C.

4.4.2 Multiscale SBS Model for 3D Shape Evolution

The 3D SBS model has been extended to include the solution with diffusion layer for the simulation of 3D device fabrications [49, 50]. Figure 4.13 illustrates the extended system which consists of three parts. The lowest part is the electrode with a small feature on the surface. The adsorption, desorption, surface diffusion, and the shape evolution are simulated by the KMC method of the SBS model. The additive reactions occur on the surface.

The solution is located above the electrode, which is also simulated by the KMC method. The solution is divided into a Cartesian grid which is the same as

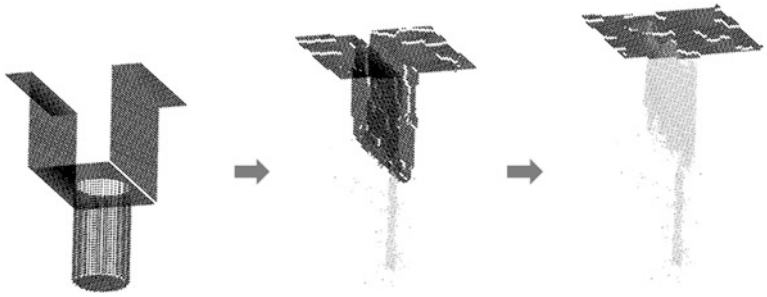

Fig. 4.12 KMC simulation of dual damascene (trench and via) using the 3D SBS basic model. *Gray dots* denote vacancies. The via is filled forming voids in the middle and then the trench is filled forming seams

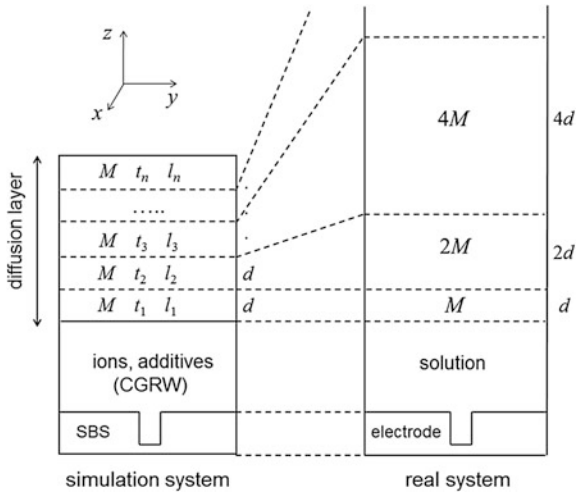

Fig. 4.13 The illustration of the multiscale modeling for electrode-solution interface. The simulation system and the corresponding real system are plotted. The system consists of the electrode, solution, and diffusion layer from the *bottom*. Multiscale method is used to simulate the diffusion layer

the cubic lattice of the SBS model for the electrode. The particles representing copper ions or additives are distributed on the grid points. The diffusion of ions and additives in solution is simulated by the coarse-grained random walk (CGRW). Ions and additives jump to one of the neighboring grid points with equal probability (1/6 for cubic lattice). Since the elementary process of ionic migration (jump diffusion) is the fastest process in the system, coarse-graining is applied, i.e., the jump distance per one KMC step is larger than the unit space of the grid.

The upper part of the solution is the diffusion layer which contains ions and additives. The migration of these particles is simulated by CGRW. Figure 4.13 shows the relation between the simulation system and the corresponding real system. The simulation system is divided into layers with the thickness d and each layer has different units of time t_j and length l_j, where j denotes the layer number. These units are scaled so that each layer corresponds to the real system which has a

larger volume with the same concentration. For example, layer 2 represents a portion of the solution with thickness $2d$ (i.e., the volume is twice as large as that of layer 1). The units t_j and l_j are scaled so that each layer has the same diffusion constant for each species. It is also assumed that each layer in the simulation system has M particles and a particle in the upper layer $j+1$ represents two particles in the lower layer j. The rate constants of the random walk of these particles at the boundary are scaled so that the microscopic detailed balance is satisfied between the layers. The whole system is simulated by the combined algorithm of the BKL method and CGRW.

The reactions in Table 4.1 have been incorporated in the 3D SBS model for copper electrodeposition. The solution contains three kinds of ion (Cu^{2+}, Cu^{+}, Cl^{-}), PEG and SPS. The reduction of Cu^{2+} occurs in two steps (reactions 1 and 2). The additive reactions 5–13 are assumed to occur on the electrode surface. Levelers are not included. The initial concentrations of ions and additives are Cu^{2+}; 2 M, Cl^{-}; 1.5×10^{-3} M, PEG; 8.8^{-5} M and SPS; 2.0^{-5} M. Surface sites are either of Cu (adatom), Cu (crystal), CuCl, CuClPEG, or Cu(I)thiolate. The inhibiting effect of PEG is simulated by the action range model in Fig. 4.8b. The catalytic effect of Cu(I)thiolate is reaction 13, which enhances copper deposition. The rate constants are taken from Refs. [38, 39]. In the simulation, the superparticle assumption is used, i.e., one lattice site represents a group of 10,648 atoms, and the rate constants are rescaled for superparticles. In this system, since the number of particles is conserved including incorporation and desorption, the effect of area change at the bottom of the trench is included. Therefore, no additional assumption is made to include the effect of area reduction.

Figure 4.14 shows the shape evolution during trench filling. The width of the trench is 132 [nm] and the aspect ratio is 2. The trench is filled from the bottom and a typical U-shape is observed during filling. As a result, only point defects appear in the film. Figure 4.15 shows the distribution of CuClPEG and Cu(I)thiolate within the trench averaged over the initial 30 % of the total filling time. $z = 0$ is the trench bottom and $z = 264$ [nm] is the initial trench top. It is clearly observed that CuClPEG is distributed at the upper half of the trench, preventing copper deposition around the opening of the trench. The accelerant Cu(I)thiolate is mainly distributed around the trench bottom. Such a heterogenous distribution of suppressors and accelerants initiates the U-shape of the surface, which leads to superfilling combined with area reduction at the bottom as observed in Fig. 4.14. These features agree with the results of the KMC-continuum simulation presented in Sect. 4.3.

4.5 Further Development of Efficient Algorithms

The numerical simulations of the continuum models and the KMC method are useful means to predict the optimal conditions in electrochemical engineering. However, accurate computation requires long computing time (more than days),

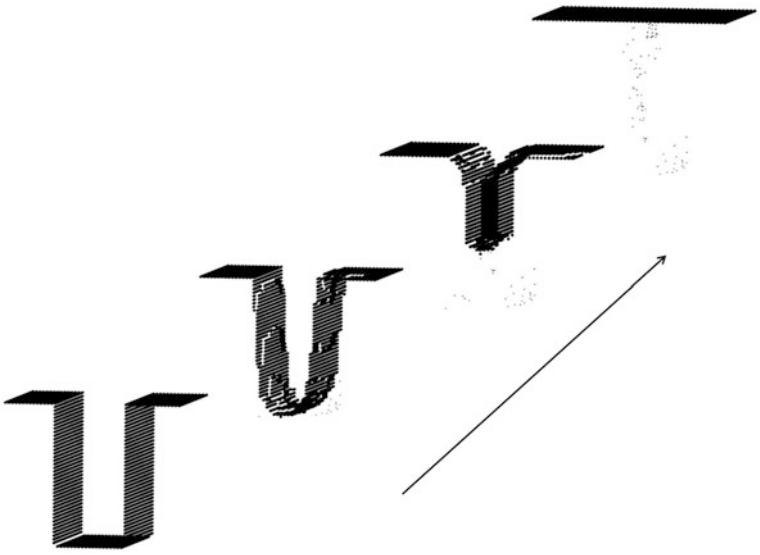

Fig. 4.14 Results of the simulation of trench filling with three additives (PEG, SPS, Cl^-). The trench is 132 [nm] wide and 264 [nm] deep. Only point defects appear in the film

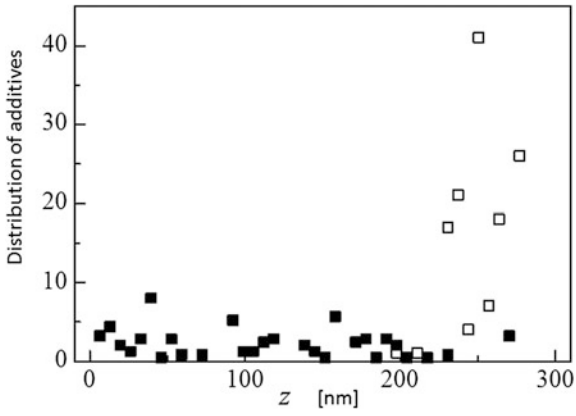

Fig. 4.15 Spatial distribution of additives averaged over the initial 30 % of the filling time (arbitrary unit). $z = 0$ is the trench bottom and $z = 264$ [nm] corresponds to the initial trench top. (*solid squares* : Cu(I)thiolate, *open squares* : CuClPEG)

especially for 3D systems, which will be the bottleneck for practical applications. Fast computing techniques have been developed for the simulations presented in the previous sections.

In the simulation of the continuum models, the large computing cost is in solving the mass balance equation (4.32) on irregular domains with moving boundaries. Buoni and Petzold [51] reported an efficient method to solve Eq. (4.32), which is an extension of the FV code. It uses FV spatial discretization including uniform small-cell region (around the feature and the electrode

boundary) and nonuniform large-cell region for the solution far from the electrode. The time integration is performed with a splitting technique. The right-hand side of Eq. (4.32) is split into three sets of terms; reaction terms, diffusion terms (plus boundary flux terms), and migration terms. The concentration field C_i is integrated in turn. It has been shown that the new algorithm is stable, scalable, and easy to parallelize. By using this method, Buoni and Petzold extended the combined system of the mass balance equation (4.32), LSM and the reaction-advection equation to a 3D system and performed the simulation of dual damascene with four kinds of additives [52].

In the KMC simulations of electrodeposition, a heavy computing cost arises when the rate of surface diffusion is much larger than the rates of other reactions. This is because numerous hops of adatoms must be computed before nucleation occurs in the ordinary KMC algorithm. The coarse-graining method (superparticles) allows us to perform the computation on large scales with the cost of losing the atomic-scale accuracy of the nucleation process. Several kinds of multiscale techniques have been developed to speed up the KMC code [33, 53].

A useful technique to overcome the problem of fast surface diffusion will be the first-passage kinetic Monte Carlo (FPKMC) method originally proposed as an efficient algorithm for the diffusion–reaction processes [54, 55]. Instead of simulating a lot of small hops, the FPKMC algorithm propagates the diffusing particles over a long distance sampled from the first-passage time distribution function which is a time-dependent Green's function of diffusion equation. The FPKMC method is an exact and efficient algorithm to skip the sampling of small hops to move the diffusing particles, which greatly reduces the computation time. Bezzola et al. applied the FPKMC method to the problem of nucleation and growth on the surface to study the presence of the exclusion zone in front of the growing step edge as a function of the surface diffusion/deposition rate ratio [56].

4.6 Summary

In this chapter, recent developments in the mathematical modeling and computer simulation of copper electrodeposition have been reviewed focusing attention on continuum models and KMC.

We first overviewed the numerical simulation of continuum models. As mathematical models for superfilling, we described the idea of the diffusion–consumption theory and the CEAC mechanism with the mathematical formulas. The CEAC is a model to realize superfilling and is regarded as a new type of leveling theory in view of accelerators. The numerical simulation of nucleation and growth and a fluid mechanical approach to copper electrodeposition are also overviewed. We then described the KMC method and the multiscale KMC-continuum simulation. The KMC-continuum hybrid method enables us to treat electrochemical phenomena ranging from microscopic surface reactions to large-scale mass transport in the diffusion layer. The recent development of the KMC method

is also presented from a "Solid-by-Solid" point of view. The extension from the SOS model to SBS model has led to a wide range of applications, especially, to the simulation of the 3D shape evolution for nanofabrication. Efficient algorithms for the fast computing of the above-mentioned simulations have also been overviewed.

Finally, let us comment on the molecular dynamics (MD) simulation which is not covered in this article. The MD method is a powerful tool to study the dynamical properties of condensed matter systems. The classical MD method, however, cannot be used for the electrochemical phenomena since the latter includes electron transfer reactions, which are essentially quantum mechanical processes. Recently a new method of molecular simulation of electrodeposition has been developed by combining the MD method with the KMC method [57, 58]. In the MD-KMC hybrid simulation, the whole dynamics of solution-electrode interface are simulated by the MD method and the reactions on the electrode are simulated by the KMC method. This method provides a direct dynamical simulation accompanying chemical reactions to study the correlation between the reaction rates and the surface morphology taking into account all the dynamics in solution and on the electrode.

The combination of efficient algorithms on different scales is the key factor in fast and accurate simulation. The simulations presented in this chapter and their hybridization will be promising tools for understanding the fundamental aspects of copper electrodeposition as well as their application to nanofabrication in electrochemical engineering.

A.1 Appendix A Level Set Method

LSM is a tracking method of moving boundaries, which is commonly used in recent numerical studies of electrodeposition. The level set function ϕ_L is a continuous function of space and time, defined in the whole area of liquid–solid interface. The surface is defined by $\phi_L = 0$, and the inner space (electrode) by $\phi_L < 0$ and the outer space (solution) by $\phi_L > 0$. The time derivative of ϕ_L is

$$\frac{\partial \phi_L}{\partial t} = \mathbf{v} \cdot \nabla \phi_L, \tag{A.1}$$

where $\mathbf{v}$ is the surface front velocity. The normal vector on the surface is:

$$\mathbf{n} = \frac{\nabla \phi_L}{|\nabla \phi_L|}, \tag{A.2}$$

and the normal velocity is defined as:

$$v = \mathbf{v} \cdot \mathbf{n}. \tag{A.3}$$

Using Eqs.(A.2) and (A.3), Eq.(A.1) becomes

$$\frac{\partial \phi_{\mathrm{L}}}{\partial t} = v|\nabla \phi_{\mathrm{L}}|. \tag{A.4}$$

The curvature of the surface in LSM is given by $\kappa = \nabla \cdot \mathbf{n}$. Equation (A.4) is the basic equation of LSM which should be solved numerically. Since v is defined not only at the interface but outside the interface, the extension velocity v_{ext} is defined by:

$$\nabla v_{\mathrm{ext}} \cdot \nabla \phi_{\mathrm{temp}} = 0, \tag{A.5}$$

where $v = v_{\mathrm{ext}}$ at $\phi_{\mathrm{L}} = 0$ and ϕ_{temp} is calculated by using the condition

$$|\nabla \phi_{\mathrm{L}}| = 1. \tag{A.6}$$

Using v_{ext} the LSM equation is written as:

$$\frac{\partial \phi_{\mathrm{L}}}{\partial t} = v_{\mathrm{ext}}|\nabla \phi_{\mathrm{L}}| \tag{A.7}$$

which is solved with the equations representing the electrodeposition reactions on the surface which give the boundary conditions. The equations are discretized and the quantities are evaluated on the grid points. The method of discretization and numerical procedures of LSM in combination with the FV code are found in the literature [9, 22].

A.2 Appendix B Rejection-Free Algorithm for KMC Simulation

Here we describe the application of the rejection-free algorithm to the 2D SOS and SBS models. Three events are assumed to occur on the surface. The rate constants for adsorption k_n^+, desorption k_n , and surface diffusion k_{nm} are dependent upon the number of nearest neighbor solid atoms n, m at the sites, where $1 \leq n, m \leq 4$. The rates of the creation (adsorption), annihilation (desorption), and surface diffusion are defined as

$$k_c = \sum_{n=1}^{3} k_n^+ N_{c(n)}, k_a = \sum_{n=1}^{3} k_n N_{a(n)}, k_d = \sum_{n,m=1}^{3} k_n N_{d(nm)}, \tag{B.1}$$

respectively, where $N_{c(n)}$, $N_{a(n)}$, $N_{d(nm)}$ are the numbers of candidate atoms (sites) for the events. The rate at which one of the three events occurs is given by

$$k_t = k_c + k_a + k_d. \tag{B.2}$$

The KMC algorithm for this model is as follows.

Search and tabulate the candidate surface atoms (sites) for the events.
Choose one of the events using a random number R on [0,1].

$$R < \frac{k_c}{k_t} \text{ : adsorption}$$

$$\frac{k_c}{k_t} \leq R < \frac{k_c + k_a}{k_t} \text{ : desorption}$$

$$\frac{k_c + k_a}{k_t} \leq R \text{ : surface diffusion}$$

Choose the type of events (the number of bonds) by generating another random number R'. In the case of adsorption,

$$R' < \frac{k_1^+ N_{c(1)}}{k_t} : n = 1$$

$$\frac{k_1^+ N_{c(1)}}{k_t} \leq R' < \frac{k_1^+ N_{c(1)} + k_2^+ N_{c(2)}}{k_c} : n = 2$$

$$\frac{k_1^+ N_{c(1)} + k_2^+ N_{c(2)}}{k_c} \leq R' : n = 3$$

Select one atom (site) from the table of the candidates for the event chosen in 2 and 3, and realize the reaction.
Renew the table and go to 2

This cycle defines one KMC step and the average time corresponding to this cycle is $1/k_t$. Additives and their reactions are incorporated in this algorithm as additional events. The numbers of the candidates for the reactions are calculated using the concentrations, which are passed from the continuum code or the results of CGRW in solution.

A.3 Appendix C Algorithm for Searching Surface Atoms

The crucial point in the extension of the SOS model to the SBS model is an efficient and accurate algorithm for searching surface atoms. Figure A.1 illustrates an example of the algorithm for a two-dimensional model. Black and white squares denote solid and liquid sites, respectively. Vacancies are denoted by white squares. The algorithm consists of successive numbering of the squares.

From the top of the liquid sites, put "1" to the white squares successively moving down in $-y$ direction.

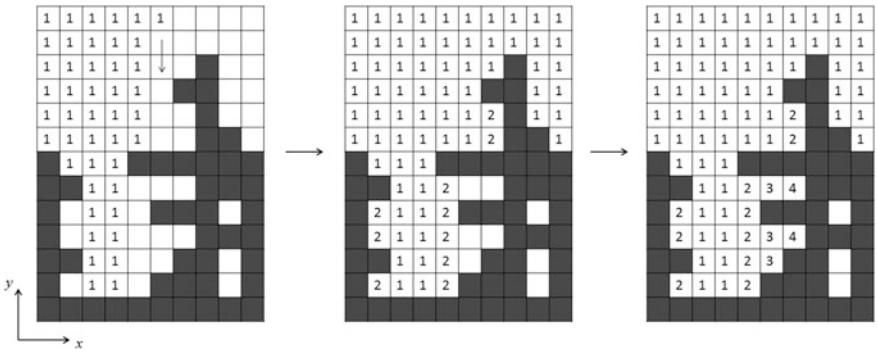

Fig. A.1 Searching algorithm of surface atoms. Successive numbering of the *squares* is illustrated. *Black squares* are solid atoms, *white squares* with numbers are liquid atoms, and *white squares* without numbers are vacancies. The surface solid atoms are the *black squares* adjacent to the numbered *white squares*

Then, put "2" to the white squares adjacent to the white squares numbered as "1".
Put "3" to the white squares adjacent to the white squares numbered as "2".
Repeat numbering the white squares adjacent to the already numbered squares.
Stop the numbering if there is no white square without numbers around the numbered white squares.
The solid squares adjacent to the "numbered" white squares are surface solid atoms. White squares adjacent to the surface solid squares are surface liquid sites.

Since the white squares surrounded by solid squares are not numbered, the liquid sites and vacancies are distinguished. It is straightforward to extend this method to a 3D model.

References

1. Andricacos PC, Uzoh C, Dukovic JO, Horkans J, Deligianni H (1998) Damascene copper electroplating for chip interconnects. IBM J Res Develop 42:567–574
2. Dukovic JO, Tobias CW (1990) Simulation of leveling in electrodeposition. J Electrochem Soc 137:3748–3755
3. Dukovic JO (1993) Feature-scale simulation of resist-patterned electrodeposition. IBM J Res Develop 37:125–141
4. West AC (2000) Theory of filling of high-aspect ratio trenches and vias in presence of additives. J Electrochem Soc 147:227–232
5. Georgiadou M, Veyret D, Sani RL, Alkire RC (2001) Simulation of shape evolution during electrodeposition of copper in the presence of additive. J Electrochem Soc 148:C54–C58
6. Josell D, Wheeler D, Huber WH, Moffat TP (2001) Superconformal electrodeposition in submicron features. Phys Rev Lett 87:016102-1–016102-4
7. Moffat TP, Wheeler D, Huber WH, Josell D (2001) Superconformal electrodeposition of copper. Electrochem Solid-State Lett 4:C26–C29

8. West AC, Mayer S, Reid J (2001) A superfilling model that predicts bump formation. Electrochem Solid-State Lett 4:C50–C53
9. Wheeler D, Josell D, Moffat TP (2003) Modeling superconformal eletrodeposition using the level set method. J Electrochem Soc 150:C302–C310
10. Wheeler D, Moffat TP, McFadden GB, Coriell S, Josell D (2004) Influence of a catalytic surfactant on roughness evolution during film growth. J Electrochem Soc 151:C538–C544
11. Josell D, Moffat TP, Wheeler D (2007) Superfilling when adsorbed accelerators are mobile. J Electrochem Soc 154:D208–D214
12. Moffat TP, Wheeler D, Edelstein MD, Josell D (2005) Superconformal film growth: mechanism and quantification. IBM J Res Develop 49:19–36
13. Moffat TP, Wheeler D, Kim SK, Josell D (2006) Curvature enhanced adsorbate coverage model for electrodeposition. J Electrochem Soc 153:C127–C132
14. Moffat TP, Wheeler D, Kim SK, Josell D (2007) Curvature enhanced adsorbate coverage mechanism for bottom-up superfilling and bump control in damascene processing. Electrochim Acta 53:145–154
15. Akolkar R, Landau U (2004) A time-dependent transport-kinetics model for additive interactions in copper interconnect metallization. J Electrochem Soc 151:C702–C711
16. Akolkar R, Landau U (2009) Mechanistic analysis of the "bottom-up" fill in copper interconnect metallization. J Electrochem Soc 156:D351–D359
17. Cao Y, Searson PC, West AC (2001) Direct numerical simulation of nucleation and three-dimensional, diffusion-controlled growth. J Electrochem Soc 148:C376–C382
18. Cao Y, West AC (2002) Nucleation and three-dimensional growth: deviation from diffusion control. J Electrochem Soc 149:C223–C228
19. Zheng M, West AC (2004) Simulation of the influence of reactant depletion on nucleation rate in electrodeposition. J Electrochem Soc 151:C502–C507
20. Emekli U, West AC (2010) Electrochemical nucleation of copper: the effect of Poly(ethylene glycol). J Electrochem Soc 157:D257–D263
21. Emekli U, West AC (2010) Simulation of the effect of additives on electrochemical nucleation. J Electrochem Soc 157:D479–D485
22. Emekli U, West AC (2010) Simulation of electrochemical nucleation in the presence of additives under galvanostatic and pulsed plating conditions. Electrochimca Acta 56:977–984
23. Stephens RM, Alkire RC (2009) Island dynamics algorithm for kinetically limited electrochemical nucleation of copper with additives onto a foreign substrate. J Electrochem Soc 156:D28–D35
24. Stephens RM, Willis M, Alkire RC (2009) Additive-assisted nucleation and growth by electrodeposition II. Mathematical model and comparison with experimental data. J Electrochem Soc 156:D28–D35
25. Alkire RC, Deligianni H (1988) The role of mass transport on anisotropic electrochemical pattern etching. J Electrochem Soc 135:1093–1100
26. Alkire RC, Deligianni H, Ju J-B (1990) Effect of fluid flow on convective transport in small cavities. J Electrochem Soc 137:818–824
27. Georgiadou M, Alkire RC (1994) Anisotropic chemical pattern etching of copper foil III. mathematical model. J Electrochem Soc 141:679–689
28. Shin CB, Economou DJ (1991) Forced and natural convection effects on the shape evolution of cavities during wet chemical etching. J Electrochem Soc 138:527–538
29. Kondo K, Fukui K, Uno K, Shinohara K (1996) Shape evolution of electrodeposited copper bumps. J Electrochem Soc 143:1880–1886
30. Kondo K, Shinohara K, Fukui K (1996) Shape evolution of higher density interconnection bumps used for microprocessor. Kagaku-kougaku Ronbunsyu 22:534–541 (in Japanese)
31. Kondo K, Fukui K, Yokoyama M, Shinohara K (1997) Shape evolution of electrodeposited copper bumps with high Peclet number. J Electrochem Soc 144:468–470
32. Kondo K, Fukui K (1998) Current evolution of electrodeposited copper bumps with photoresist angle. J Electrochem Soc 145:840–884

33. Chatterjee A, Vlachos DG (2007) An overview of spatial microscopic and accelerated kinetic Monte Carlo methods. J Computer-Aided Mater Des 14:253–308
34. Drews TO, Krishnan S, Alameda Jr JC, Gannon D, Braatz RD, Alkire RC (2005) Multiscale simulations of copper electrodeposition onto a resistive substrate. IBM J Res Develop 49:49–63
35. Pricer TJ, Kushner MJ, Alkire RC (2002) Monte Carlo simulation of the electrodeposition of copper I. Additive-free acidic sulfate solution. J Electrochem Soc 149:C396–C405
36. Drews TO, Ganley JC, Alkire RC (2003) Evolution of surface roughness during copper electrodeposition in the presence of additives—Comparison of experiments and Monte Carlo simulations. J Electrochem Soc 150:C325–C334
37. Drews TO, Radisic A, Erlebacher J, Braatz RD, Searson PC, Alkire RC (2006) Stochastic simulation of the early stages of kinetically limited electrodeposition. J Electrochem Soc 153:C434–C441
38. Li X, Drews TO, Rusli E, Xue F, He Y, Braatz RD, Alkire RC (2007) Effect of additives on shape evolution during electrodeposition I. Multiscale simulation with dynamically coupled kinetic Monte Carlo and moving-boundary finite-volume codes. J Electrochem Soc 154:D230–D240
39. Rusli E, Xue F, Drews TO, Vereecken PM, Andricacos P, Deligianni H, Braatz RD, Alkire RC (2007) Effect of additives on shape evolution during electrodeposition II. Parameter estimation from roughness evolution experiments. J Electrochem Soc 154:D584–D597
40. Qin Y, Li X, Xue F, Vereecken PM, Andricacos P, Deligianni H, Braatz RD, Alkire RC (2008) Effect of additives on shape evolution during electrodeposition III. Trench infill for on-chip interconnects. J Electrochem Soc 155:D223–D233
41. Gilmer GH, Bennema P (1972) Computer simulation of crystal surface structure and growth kinetics. J Cryst Growth 13(14):148–153
42. Gilmer GH, Bennema P (1972) Simulation of crystal growth with surface diffusion. J App Phys 43:1347–1360
43. Bortz AB, Kalos MH, Lebowitz JL (1975) A new algorithm for Monte Carlo simulation of Ising spin system. J Comp Phys 17:10–18
44. Gillespie DT (1976) A general method for numerically simulating the stochastic time evolution of couples chemical reactions. J Comp Phys 22:403–434
45. Kaneko Y, Hiwatari Y, Ohara K, Murakami T (2000) Monte Carlo simulation of thin film growth with lattice defects. J Phys Soc Jpn 69:3607–3613
46. Kaneko Y, Hiwatari Y (2002) The solid-by-solid model for crystal growth and electroplating: kinetic Monte Carlo simulation. In: Pandalai SG (ed) Recent research developments of physics and chemistry of solids, vol 1. Transworld Research Network, India p 47–64
47. Kaneko Y, Hiwatari Y, Ohara K (2004) Monte Carlo simulation of thin film growth with defect formation : application to via filling. Mol Sim 30:895–899
48. Kaneko Y, Hiwatari Y, Ohara K, Asa F (2006) Monte Carlo simulation of damascene electroplating: effects of additives. Mol Sim 32:1227–1232
49. Kaneko Y, Hiwatari Y, Ohara K, Asa F (2010) Simulation of three-dimensional solid-by-solid model and application to electrochemical engineering. ECS Trans 28(29):1–7
50. Kaneko Y, Hiwatari Y, Ohara K, Asa F (2011) Kinetic Monte Carlo approach to the effects of additives in electrodeposition. ECS Trans 35(27):7–12
51. Buoni M, Petzold L (2007) An efficient, scalable numerical algorithm for the simulation of electrochemical systems on irregular domains. J Comp Phys 225:2320–2332
52. Buoni M, Petzold L (2010) An algorithm for simulation of electrochemical systems with surface–bulk coupling strategies. J Comp Phys 229:379–398
53. Chatterjee A, Vlachos DG (2006) Multi-scale Monte Carlo simulations: multigriding, computational singular perturbation, and hierarchical stochastic closure. J Chem Phys 124:064110-1–064110-16
54. Oppelstrup T, Bulatov VV, Gilmer GH, Kalos MH, Sadigh B (2006) First-passage Monte Carlo algorithm: diffusion without all the hops. Phys Rev Lett 97:230602-1–230602-4

55. Oppelstrup T, Bulatov VV, Donev A, Kalos MH, Gilmer GH, Sadigh B (2009) First-passage kinetic Monte Carlo method. Phys Rev E 80:066701-1–066701-14
56. Bezzola A, Alkire RC, Petzold L (2012) Multiscale stochastic simulation of surface diffusion during early stages of electrodeposition, 221th ECS Meeting Abstract, **2012**., Abstract #1031
57. Hiwatari Y, Kaneko Y, Mikami T, Ohara K, Asa F (2007) Molecular dynamics-Monte Carlo hybrid simulation of thin film growth and void formation in electrodeposition process. Mol Sim 33:133–138
58. Kaneko Y, Nishimura S, Hiwatari Y, Ohara K, Asa F (2009) Monte Carlo and molecular dynamics studies of the effects of additives in electrodeposition. J Korean Phy Soc 54:1207–1211